

Article

A Trinuclear Co(II) Complex Based on the Tris-Dioxolene Triphenylene Non-Innocent Bridge: Complementary Redox, Magnetic Behavior and Theoretical Calculations †

Aristide Colin ¹, Yiting Wang ¹, François Lambert ¹, Nathalie Bridonneau ^{1,*}, Nicolas Suaud ^{2,*}, Régis Guillot ¹, Eric Rivière ¹, Zakaria Halime ¹, Nathalie Guihéry ², Shin-ichi Ohkoshi ³ and Talal Mallah ^{1,*}

¹ Institut de Chimie Moléculaire et des Matériaux d'Orsay, CNRS, Université Paris-Saclay, 17, Avenue des Sciences, 91400 Orsay, France; aristide.colin@universite-paris-saclay.fr (A.C.); yitingwang527829@outlook.com (Y.W.); francois.lambert.saclay@gmail.com (F.L.); regis.guillot@universite-paris-saclay.fr (R.G.); eric.riviere@universite-paris-saclay.fr (E.R.); zakaria.halime@universite-paris-saclay.fr (Z.H.)

² Laboratoire de Chimie et Physique Quantiques (LCPQ), Université de Toulouse, CNRS, 118 Route de Narbonne, 31062 Toulouse, France; nathalie.guihery@irsamc.ups-tlse.fr

³ Department of Chemistry, School of Science, The University of Tokyo, 7-3-1 Hongo, Bunkyo-ku, Tokyo 113-0033, Japan; ohkoshi@chem.s.u-tokyo.ac.jp

* Correspondence: nathalie.bridonneau@universite-paris-saclay.fr (N.B.); suaud@irsamc.ups-tlse.fr (N.S.); talal.mallah@universite-paris-saclay.fr (T.M.)

† This article is dedicated to the long and outstanding scientific careers of Miguel Julve and Paco Lloret, two pioneers in the fields of coordination chemistry and magnetochemistry, two friends whose collaboration over more than 40 years impacted the domain of molecular magnetism and is an example for the young generation. Sadly, Miguel left us on 9 July 2024. We have not only lost a brilliant chemist and colleague, an outstanding teacher, highly esteemed by his students and his collaborators all over the world and particularly in France, but, even more, a close friend with a fine sense of humor, a fast mind and a generosity that we will never forget.



Citation: Colin, A.; Wang, Y.; Lambert, F.; Bridonneau, N.; Suaud, N.; Guillot, R.; Rivière, E.; Halime, Z.; Guihéry, N.; Ohkoshi, S.-i.; et al. A Trinuclear Co(II) Complex Based on the Tris-Dioxolene Triphenylene Non-Innocent Bridge: Complementary Redox, Magnetic Behavior and Theoretical Calculations. *Magnetochemistry* **2024**, *10*, 102. <https://doi.org/10.3390/magnetochemistry10120102>

Academic Editors: Carlos J. Gómez García and Salah-Eddine Stiriba

Received: 25 November 2024

Revised: 6 December 2024

Accepted: 9 December 2024

Published: 11 December 2024



Copyright: © 2024 by the authors. Licensee MDPI, Basel, Switzerland. This article is an open access article distributed under the terms and conditions of the Creative Commons Attribution (CC BY) license (<https://creativecommons.org/licenses/by/4.0/>).

Abstract: A trinuclear Co(II)-containing complex was assembled using the non-innocent hexahydroxytriphenylene bridging ligand. Cyclovoltammetry and spectroelectrochemistry studies revealed that the central ligand sustained four reversible redox events, leading to different species with diverse optical behavior. Complementary analysis of the molecular structure confirmed by ab initio theoretical calculations were consistent with the bridge in the tris-semiquinone (sq) state for the trinuclear complex. The exchange coupling among the electrons of the bridge resulted in a spin doublet ($s = 1/2$) localized close to one of the three Co^{2+} ions, as suggested by the experimental magnetic data. The central doublet underwent one large antiferromagnetic exchange coupling with one Co(II) and almost no coupling with the two other metal ions.

Keywords: hexahydroxytriphenylene; non-innocent bridge; trinuclear Co complex; spectroelectrochemistry; Co magnetism; ab initio calculations

1. Introduction

Hexahydroxytriphenylene (noted H_6HHTP ; $\text{C}_{18}\text{O}_6\text{H}_{12}$, Figure 1a) may, when deprotonated, present seven oxidation states from the fully reduced tris catecholate (HHTP^{6-} ; [cat-cat-cat]) to the fully oxidized tris quinone (HHTP ; [q-q-q]), as has been shown by Ward et al., when the ligand bridges Ru(II)-containing complexes [1–3]. However, this non-innocent redox active ligand was used only recently for the design of polynuclear complexes with magnetic ions, therefore adding a new functionality and providing original multifunctional polynuclear complexes. The trinuclear complexes were prepared with first row transition paramagnetic metal ions (Ni^{2+} and Cu^{2+}) [4–7]. For all these molecules, the most stable state of the bridging HHTP is [sq-sq-sq] (sq = semiquinone). In our effort to understand the electronic and magnetic behavior of these complexes, we have shown that,

because the bridging ligand adopts the mesomeric form $\text{HHTP}^{3- -1}$ (Figure 1b) instead of a three-fold symmetry axis ($\text{HHTP}^{3- -2}$, Figure 1c), the interaction between the three unpaired sq electrons stabilizes a doublet ground state ($s = 1/2$) that is mainly localized on one of the OCCO dioxolene moieties, leading to a large antiferromagnetic exchange coupling with one of the Ni^{2+} metal ions, and one ferro- and one antiferromagnetic coupling with the other two Ni^{2+} , of weaker magnitudes [7]. Both experimental data (structure and magnetic) and *ab initio* theoretical calculations supported this view of the electronic structure, independently from the nature of the metal ions and from their geometry that can be a distorted octahedron, a distorted square pyramid or a distorted trigonal bipyramid [7].

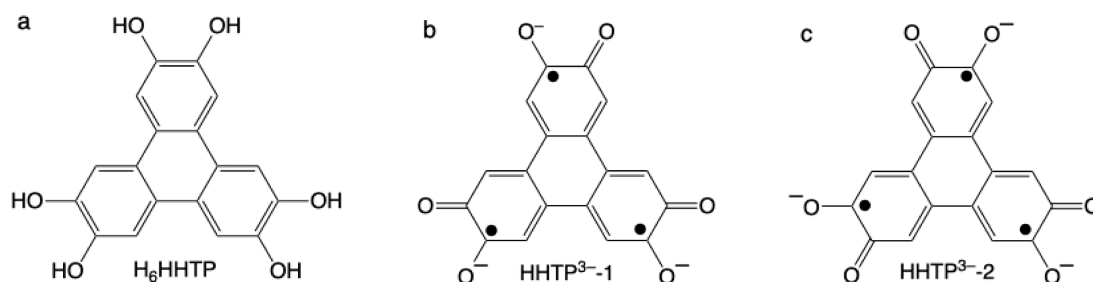


Figure 1. Chemical formula for H_6HHTP (a), the mesomeric form of the tris-semiquinone state HHTP^{3-} that lacks three-fold symmetry axis (b), and the mesomeric form of the tris-semiquinone with a three-fold symmetry axis (c).

The aim of this article was (i) to extend our study to a trinuclear complex with the paramagnetic Co^{2+} metal ions ($s = 3/2$) where each metal center possesses three unpaired electrons, (ii) to verify whether the tris-semiquinone state remains the most stable and (iii) to assess to which extent the presence of Co^{2+} instead of Ni^{2+} metal ions affects the electronic structure of the HHTP, the exchange coupling within the complex, the redox and the optical behaviors. A trinuclear complex containing Co was reported but the metal ions were diamagnetic in the oxidation state III, probably because the capping tetradentate ligand imposes a strong ligand field that stabilizes Co(III) [8]. We therefore used $[\text{Co}(\text{BH}(\text{Tp}^{\text{Ph,Ph}})_3)]^+$, (where $\text{BH}(\text{Tp}^{\text{Ph,Ph}})_3$ is the tris(3,5-diphenyl-1H-pyrazol-1-yl)(hydridoborate)), as a building block with a tridentate capping ligand that induces a relatively weak ligand field and is expected to stabilize Co(II) in the high spin state [9].

We report the preparation (details of the synthesis and full characterization are given in SI), the crystal structure, the redox, the optical and the magnetic behavior of the trinuclear complex of formula $[\text{HHTP}(\text{Co}(\text{BH}(\text{Tp}^{\text{Ph,Ph}})_3))]^+$ noted Co_3HHTP in the following. *Ab initio* calculations were also carried out in order to determine the electronic structure of the complex and to facilitate the analysis of its magnetic properties.

2. Materials and Methods

2.1. Cyclic Voltammetry

The cyclic voltammetry experiments were carried out on solutions of 1 mM of the complex dissolved in dichloromethane with $(\text{NBu}_4)\text{PF}_6$ at 0.1 M as supporting electrolyte. The potentiostat was an AUTOLAB PGSTAT320 from Metrohm Autolab, and the three-electrode setup comprised a glassy carbon working electrode ($\text{Ø} = 1\text{mm}$), a platinum wire as counter electrode and a saturated calomel electrode as reference. Ferrocene was used as an internal reference and the presented voltammogram was acquired with a voltage sweeping speed of 100 mV/s.

2.2. Spectroelectrochemistry

UV–vis–NIR spectra were recorded using a Cary 5000 UV–vis–NIR spectrometer from Varian (Palo Alto, CA, USA) in double beam mode. Quartz cuvettes of 1 cm optical path length were used. For the spectroelectrochemical tandem measurements, the Varian Cary 5000 UV–vis–NIR spectrometer (Palo Alto, CA, USA) was used in single beam mode. The

cuvette from Pine Research was made out of quartz and had a 1.7 mm optical path length. A combined platinum electrode was used as a counter and working electrode as well as reference electrode. The working electrode was of mesh-type. For reduction experiments, an argon flux was adapted on the cuvette in order to perform the reduction under a controlled atmosphere. The applied voltage was delivered by an Autolab PGSTAT204 potentiostat from Metrohm Autolab; Villebon Courtaboeuf, France.

2.3. Magnetic Measurements

The magnetic data were acquired using a MPMS XL7 Quantum Design SQUID magnetometer (San Diego, CA, USA) operating in the 2–300 K temperature range and in the 0–6 T field range. Crystalline powder of Co₃HHTP was ground and a pellet was made in order to prevent torquing effects at low temperatures and high magnetic fields. Diamagnetic correction of the sample holder, and of the compound using a Pascal scheme, were performed.

2.4. Preparation of the Different Compounds

The synthesis and full characterization of the precursors and of Co₃HHTP are given in Supplementary Materials.

2.5. Single Crystal X-Ray Diffraction

X-ray diffraction data for Co₃HHTP were collected by using a VENTURE PHOTON 100 Bruker diffractometer (Billerica, MA, USA) with Micro-focus IuS source Mo-K α radiation. The crystal of the compounds was selected under an optical microscope and glued in paratone oil. The crystal was mounted on a CryoLoop (Hampton Research; Aliso Viejo, CA, USA) with Paratone-N (Hampton Research) as cryoprotectant and then placed in a nitrogen-gas stream at low temperature. The temperature of the crystal was maintained at the selected value by means of a cooling device by a N-Helix Cryostream cooling device (Oxford Cryosystems, Long Hanborough, UK) with an accuracy of ± 1 K. Data reduction was accomplished using SAINT V7.53a. The substantial redundancy in data allowed a semi-empirical absorption correction (SADABS V2.10) to be applied on the basis of multiple measurements of equivalent reflections. The structures were solved by direct methods using SHELXS-97 [10], and refined against F^2 by full-matrix least-squares techniques using SHELXL-2018 [11], with anisotropic displacement parameters for all non-hydrogen atoms. Hydrogen atoms were introduced into the calculations as a riding model with isotropic thermal parameters. All calculations were performed by using the crystal structure crystallographic software package WINGX [12]. CCDC 2403865 contains the supplementary crystallographic data for this paper. These data can be obtained free of charge from the Cambridge Crystallographic Data Centre and Fachinformationszentrum Karlsruhe via “<http://www.ccdc.cam.ac.uk/structures/>” accessed on 9 December 2024”.

2.6. Ab Initio Calculations

Ab initio wave function-based calculations were performed using the ORCA5 code [13]. The treatment of the spin-orbit couplings (SOC) was achieved using the spin-orbit state interaction (SO-SI) method [14]. Calculations were carried out on a model complex where Co was replaced by Zn (noted Zn₃HHTP) in order to examine the electronic structure of HHTP. For this model, Def2-TZVP atomic basis sets were used for all atoms of the HHTP ligand (C and O: 5s3p2d1f) and Def2-SVP atomic basis sets for other atoms (Zn: 5s3p2d1f, B, C, N and O: 3s2p1d, H:2s1p). For Co₃HHTP, Def2-TZVP atomic basis sets were used for all atoms (Co: 6s4p4d1f, B, C, N and O: 5s3p2d1f) except H, for which Def2-SVP atomic basis sets were used (2s1p) and for the Zn₂Co1, Zn₂Co2 and Zn₂Co3 models (see Section 3.2 for the definition of these model complexes), Def2-TZVP atomic basis sets were used for the Co ions and the atoms of its coordination sphere (Co: 6s4p4d1f, N and O: 5s3p2d1f) while Def2-SVP atomic basis sets were used for other atoms (Zn: 5s3p2d1f, B, C, N and O: 3s2p1d, H: 2s1p).

3. Results and Discussion

3.1. Crystal Structure

The crystal data collection and refinement parameters for Co_3HHTP are given in Table S1. Co_3HHTP is a trinuclear complex made from the assembly of a central HHTP ligand bridging three $[\text{Co}(\text{BH}(\text{Tp}^{\text{Ph,Ph}})_3)]$ complexes through the three dioxolene groups (Figures 2 and S1).

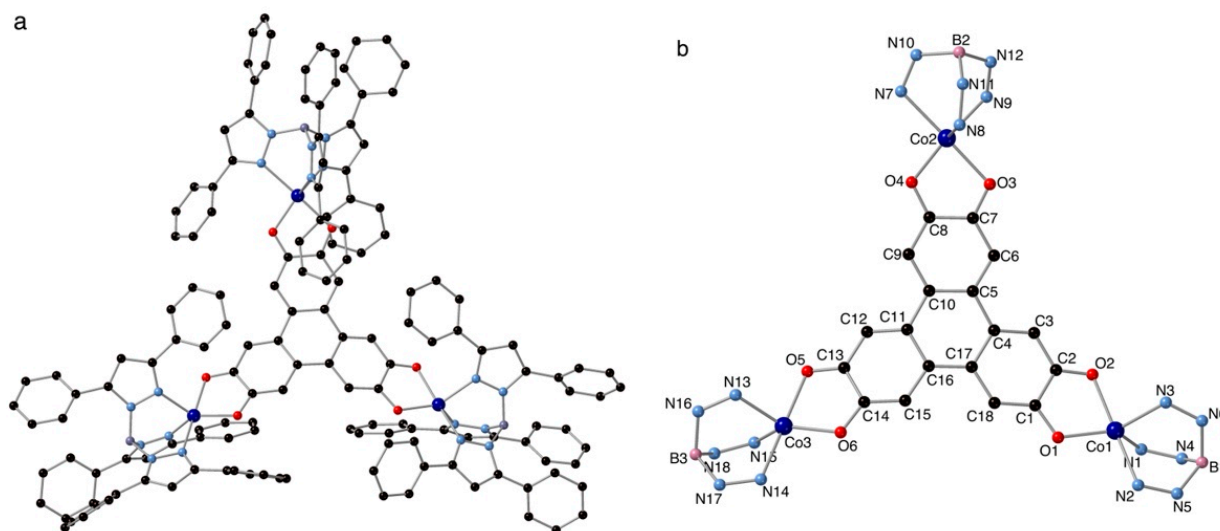


Figure 2. View of the molecular structure of Co_3HHTP (a) and with atom numbering, and with part of the peripheral tridentate ligand removed (b).

The Co atoms were pentacoordinate with a geometry close to trigonal bipyramidal (tbp; Addison parameter [15] τ close to 0.65). The pseudo three-fold symmetry axes of the three Co(II) complexes lay within the plane of the molecule and corresponded to the N2-O2, N7-O3 and N14-O5 directions for Co1, Co2 and Co3, respectively. The bond distances in the coordination sphere of the Co atoms were shorter in the tbp plane than along the pseudo three-fold axes (Table 1). The difference in the C-O bond lengths for the OCCO dioxolene moieties (Table 2) indicates that the unpaired sq electrons close to Co1 and Co3 were located on C1 and C14 (Figure 2b). For the OCCO moiety close to Co2, the difference in the C-O bond lengths was much smaller, indicating a relative delocalization of the sq unpaired electron over the OCCO moiety. The Co-O bond lengths were correlated with the C-O distances. The short Co-O bond distances were those with the oxygen atoms that had the longer C-O bonds (i.e., O1, O4 and O6 for Co1, Co2 and Co3, respectively), those that were formally negatively charged.

Table 1. Bond distances (in Å) in the coordination sphere of Co atoms for Co_3HHTP .

Co-Ligand Distances Along the Pseudo Three-Fold Axes		Co-Ligand Distances in the Equatorial Plane		
Co1-O2	Co1-N2	Co1-O1	Co1-N1	Co1-N3
2.1113(17)	2.143(2)	1.9606(18)	2.047(2)	2.042(2)
Co2-O3	Co2-N7	Co2-O4	Co2-N8	Co2-N9
2.0788(19)	2.152(2)	1.9602(18)	2.039(2)	2.032(2)
Co3-O5	Co3-N14	Co3-O6	Co3-N15	Co3-N13
2.1113(17)	2.114(2)	1.9612(19)	2.055(2)	2.039(2)

Table 2. Bond distances and their difference (in Å) for the OCCO moieties for Co₃HHTP.

C1-O1	C2-O2	$\Delta(\text{C-O})_{\text{Co1}}$
1.313(3)	1.258(3)	0.055(6)
C8-O4	C7-O3	$\Delta(\text{C-O})_{\text{Co2}}$
1.291(3)	1.280(3)	0.011(6)
C14-O6	C13-O5	$\Delta(\text{C-O})_{\text{Co3}}$
1.303(3)	1.257(3)	0.046(6)

These structural characteristics are consistent with the electronic structure of the central HHTP ligand depicted in Figure 1b, where the sq unpaired electrons of the OCCO moieties close to Co1 and Co3 are separated by 5 C-C bonds. The interaction between the three $s = \frac{1}{2}$ spins of the three sq unpaired electrons led to two doublet and one quadruplet states. The electronic structure that emerged from the crystallographic analysis should, therefore, have led to a ground doublet spin state ($s = \frac{1}{2}$) well separated in energy from the other doublet and the quadruplet states, because of a large antiferromagnetic exchange coupling between the two sq electrons separated by 5 C-C bonds. Theoretical calculations were, thus, carried out in order to confirm the electronic structure that emerged from the crystallographic structural analysis and to evaluate the exchange coupling between the central spin and those of the Co²⁺ metal ions.

3.2. Theoretical Calculations

For the ab initio wave function-based calculations on the model complex Zn₃HHTP, the orbitals were optimized at the complete active space self-consistent field CAS(3,3)SCF level with an active space containing 3 electrons in 3 HHTP orbitals. Then, calculations on a CAS(12,12) active space (12 electrons, 3 from the HHTP and 9 from the three Co(II) in 12 orbitals) were performed on the whole complex. Finally, we carried out calculations on one-electron oxidized model complexes noted as Zn₂Co1, Zn₂Co2 and Zn₂Co3, where one Zn was replaced by one Co for the three sites Co1, Co2 and Co3, respectively, with the CAS(7,5) active space involving the 7 valence electrons of each Co(II) in their 5 3d orbitals in order to determine the axial (*D*) and rhombic (*E*) zero-field splitting (ZFS) parameters of the three Co fragments corresponding to the spin Hamiltonian:

$$\hat{H}_{ZFS} = D \left[\hat{s}_z^2 - \frac{s(s+1)}{3} \right] + E (\hat{s}_x^2 - \hat{s}_y^2) \quad (1)$$

The molecular orbitals of the model complex Zn₃HHTP optimized for the doublet ground state at the CAS(3,3)SCF level showed one bonding (HOMO), one non-bonding (SOMO) and one antibonding (LUMO) orbital, as depicted in Figure 3. The SOMO (Figure 3b) was mainly localized on the OCCO moiety close to Co2 and had almost no contribution to the two other OCCO groups.

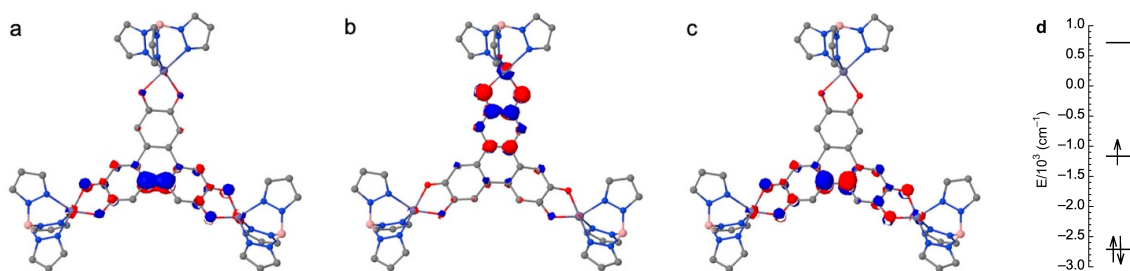


Figure 3. Frontier π orbitals HOMO (a), SOMO (b) and LUMO (c) for Zn₃HHTP computed at the CAS(3,3)SCF level with electron occupation numbers 1.91, 1.00 and 0.09, respectively, and MO energy diagram (d).

The low energy spectrum was calculated using state average CAS(3/3)SCF + NEVPT2 calculations for the 2 lowest $s = 1/2$ and the lowest $s = 3/2$ spin states. It showed a doublet ground state ($s = 1/2$), an excited doublet ($s = 1/2$) at 5144 cm^{-1} and a quadruplet ($s = 3/2$) at 5468 cm^{-1} . Enlarging the active space did not change the spectrum qualitatively: the energy of excited $s = 1/2$ and the $s = 3/2$ states with respect to the ground state were 4705 cm^{-1} and 6566 cm^{-1} , respectively, for CAS(7,7)SCF + NEVPT2 calculations. The central ligand can thus be described as having one unpaired electron ($s_L = 1/2$) expected to interact mainly with the unpaired electrons of Co2.

We then studied Co_3HHTP using a state average CAS(12,12)SCF calculation for all states generated by the interaction of three $s = 3/2$ on the Co^{2+} ions and one $s_L = 1/2$ on the bridging ligand (i.e., one $S = 5$, three $S = 4$, five $S = 3$, seven $S = 2$, six $S = 1$ and two $S = 0$ states). The obtained molecular orbital energy diagram for Co_3HHTP (Figure 4) showed three sets of orbitals: one set where the orbitals were localized only on Co(II) with no contribution on HHTP (Figure 4, blue lines and Figure S2 for orbitals representation); one set with one bonding and one antibonding MOs localized on HHTP (Figure 4, green lines) that was almost the same as those computed for Zn_3HHTP (Figure 3a,c); and one set with a bonding and an antibonding MOs involving the SOMO of HHTP and one d orbital of Co2 (Figure 4, red lines). This orbital energy diagram indicates that the electronic structure of Co_3HHTP was mainly governed by the interaction between the SOMO of HHTP and one d orbital of one of the three Co^{2+} metal ions, namely Co2. We, therefore, expected that the magnetic behavior of the trinuclear complex would be mainly governed by the exchange coupling between the spins of these two moieties, and by the local anisotropy of Co^{2+} ions that also needed to be evaluated.

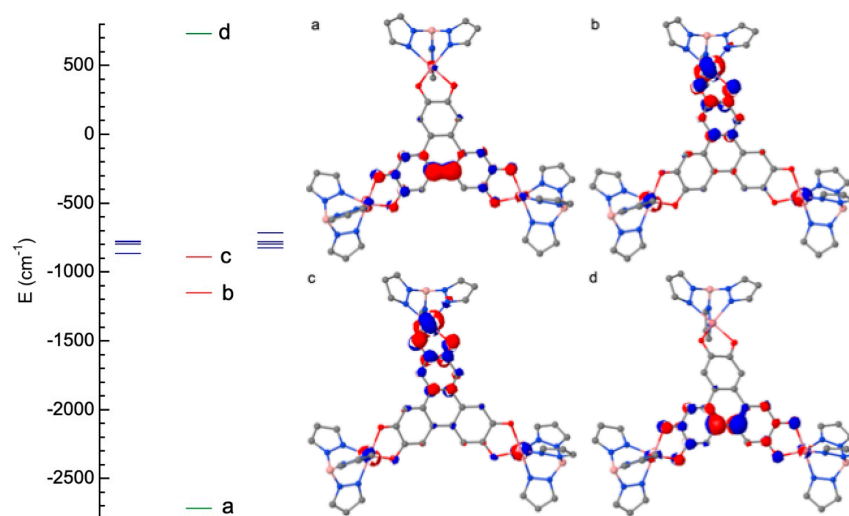


Figure 4. Energy levels of the MOs calculated for Co_3HHTP at the CAS(12,12)SCF level and representation of the MOs localized on HHTP (a,d) and of the MOs resulting from the interaction between the SOMO of HHTP and one d orbital of one Co(II) (b,c). A representation of the MOs localized on the Co atoms is given in Supplementary Materials (Figure S2).

The corresponding model Hamiltonian involves the exchange coupling parameters J_2 between the ligand doublet spin momentum \hat{s}_L and the Co2 spin momentum \hat{s}_2 and the local anisotropies of the three Co(II) species:

$$\hat{H} = -J_2 \hat{s}_L \cdot \hat{s}_2 + \sum_k \left(\hat{s}_k \cdot \overline{D}_k \cdot \hat{s}_k \right) \quad (2)$$

The CAS(12,12)SCF + NEVPT2 energy spectrum (Table S2) confirmed a strong antiferromagnetic coupling J_2 between the ligand and Co2 spins of the order of 65 cm^{-1} (see SI). It resulted in an effective local metal-ligand ground triplet state ($\hat{s}_{\text{Co}2-L} = 1$) and an excited

quintet state ($\hat{s}'_{Co2-L} = 2$). Indeed, the analysis of the spectrum showed a low energy first set of 10 quasi-degenerate states (spectrum width $\sim 7\text{cm}^{-1}$) corresponding to small couplings (few cm^{-1}) between \hat{s}_{Co2-L} and \hat{s}_1 and \hat{s}_3 , and a second set (14 states) higher in energy ($-2J_2 = 130\text{cm}^{-1}$, bandwidth $\sim 20\text{cm}^{-1}$) corresponding as well to small couplings (few cm^{-1}) between \hat{s}'_{Co2-L} and \hat{s}_1 and \hat{s}_3 .

The ZFS parameters (Table 3) were extracted using an already reported method [16]. We found relatively large negative D values for the three Co(II) fragments with a large rhombicity (we note that the maximum rhombicity corresponded to $E/|D| = 0.33$). As ZFS values were particularly large, we checked that the first-order SOC contributions were negligible. The easy axis of magnetization for the three Co(II) fragments (Figure 5) was aligned along the Co-O short bonds and not along the pseudo three-fold axis of the tbp. In order to analyze the origin of the negative D values, we focused on one Co(II) species (Co2), since the interpretation of the results was the same for the three metal ions (see Table S3 and Table S4 for the composition of the wave function of the ground and excited $s = 3/2$ states obtained from calculations on the Co1 and Co2 sites). The calculation also provided the contribution at the second order of perturbation of each excited state to the overall D value. The first excited state was mainly responsible of the large negative D values for the Co(II) species (Tables S3 and S4). If we consider the Co2 fragment, the contribution of the first excited state was found equal to -53cm^{-1} (Table S3) and corresponded to an excitation between d_{xy} and $d_{x^2-y^2}$ orbitals that are linear combinations of the $l = 2, m_l = \pm 2$ spherical harmonics, and therefore it was the $\hat{l}_z\hat{s}_z$ part of the spin-orbit operator that coupled this state to the ground state. When SO couples through $\hat{l}_z\hat{s}_z$ states of the same spin, it stabilizes the largest $|m_s|$ values ($\pm 3/2$) of the ground state and therefore contributes negatively to D [17,18]. The third excited state was obtained by an excitation between the d_{yz} and d_{xz} orbitals (linear combinations of $m_l = \pm 1$) and had, for the same reasons, a negative contribution to D but weaker in magnitude (-15.6cm^{-1} instead of -53.1cm^{-1}) because of the weaker $|m_l|$ values and to the larger energy separation with the ground state (5451cm^{-1} instead of 1138cm^{-1}). The second and the fourth excited states had positive contributions (Table S3), but of much weaker magnitude so that the overall D value remained negative and large. For Co1, the same analysis justified its negative D value (Table S4).

Table 3. Axial D and rhombic E ZFS parameters (in cm^{-1}) calculated using the SO-SI method with the CAS(7,5)NEVPT2 energies for the three Co(II) fragments.

ZFS Parameters	Co1	Co2	Co3
D	-67.1	-58.9	-63.7
E	16.4	15.2	15.5
$E/ D $	0.24	0.26	0.24

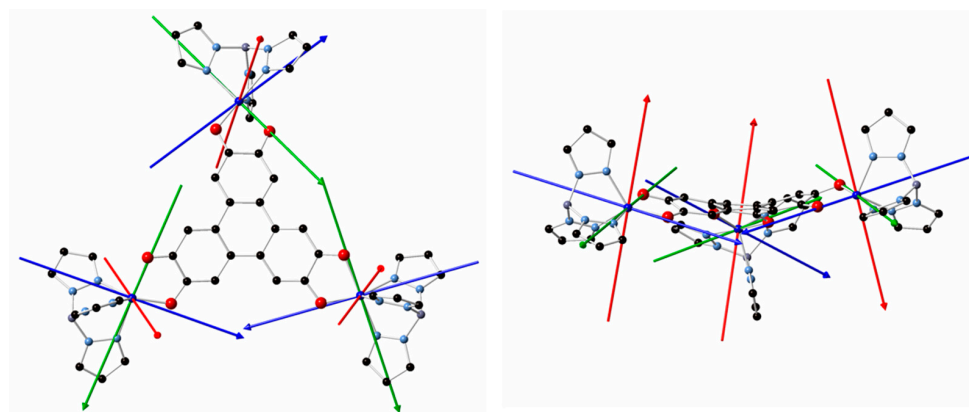


Figure 5. Relative orientation of the \bar{D} tensor axes (blue, easy axis: green, intermediate axis and red, hard axis) for the three Co moieties in Co_3HHTP .

3.3. Redox and Optical Properties

In order to investigate the redox and optical behavior of Co_3HHTP , we performed cyclic voltammetry (CV) and spectroelectrochemistry studies to evaluate the stability of the different species. Those data were compared with the previously reported Ni(II)-containing compound of general formula $[\text{HHTP}\{\text{Ni}(\text{BH}(\text{Tp}^{\text{Ph,Ph}})_3)\}]$ that possesses a similar structure with the same capping ligand (noted Ni_3HHTP in the following) and where HHTP is also in the [sq-sq-sq] state [4]. The CV of Co_3HHTP showed four reversible redox waves similar to those observed for the Ni(II) complex; three one-electron reduction waves and one one-electron oxidation wave (Figure 6, Table S5). The first reduction wave had the same redox potential as that of Ni_3HHTP , while the other waves were slightly shifted anodically, indicating a higher energy requirement for the oxidation process and more energetically accessible second and third reduction processes for Co_3HHTP compared to Ni_3HHTP . In the latter, the redox processes were mainly located on HHTP because Ni(II) is redox-inactive in the observed potential window. The very close redox potential values for Co_3HHTP indicate that the redox processes were also not metal-centered as for Ni_3HHTP and that they, therefore, mainly involved the bridging ligand HHTP.

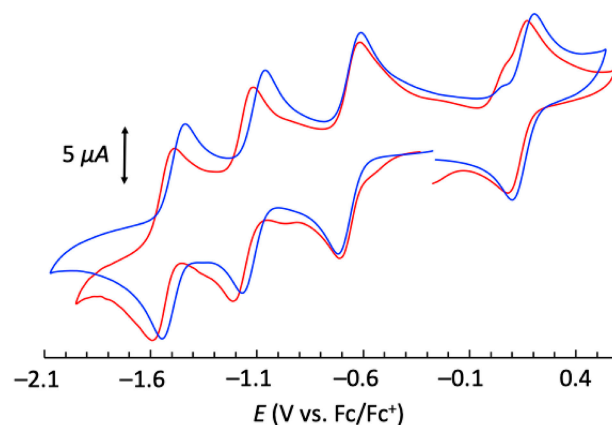


Figure 6. Cyclic voltammogram of 1 mM of Co_3HHTP (blue trace) and of Ni_3HHTP (red trace) in argon-degassed dichloromethane containing 0.1 M $[\text{Bu}_4\text{N}]\text{PF}_6$ at 25 °C and recorded using a glassy carbon working electrode, a platinum mesh as the counter electrode and a saturated calomel electrode (SCE) as the reference electrode.

The electronic spectra of Co_3HHTP as well as its one-electron reduced and one-electron oxidized analogues were recorded using UV-vis-NIR spectroelectrochemistry. The three species showed two sets of absorption bands: in the near infrared (NIR) and in the visible region (Figure 7). We focused the following on the NIR region. Co_3HHTP displayed an absorption band at 1140 nm that was red-shifted to 1315 nm (this band was probably due to two transitions at 1292 and 1370 nm) upon a one-electron reduction and blue-shifted to 1183 nm for the one-electron oxidized species. In order to propose a qualitative assignment for these bands, we compared the electronic spectra to those of Ni_3HHTP (Figure 8).

The absorption bands in the NIR region of Co_3HHTP and Ni_3HHTP (Figure 8a) were almost identical, leading to the conclusion that the nature of the metal ions had almost no effect on the electronic transitions and that, therefore, these bands were due to transition(s) within the HHTP when it was in the [sq-sq-sq] state. In fact, with this hypothesis one could expect three absorption bands for the [sq-sq-sq] HHTP based on the MOs energy diagram of the model complex Zn_3HHTP (Figure 3d), corresponding to the promotion of an electron between the three couple of MOs: $\text{HOMO} \rightarrow \text{SOMO}$, $\text{SOMO} \rightarrow \text{LUMO}$ and $\text{HOMO} \rightarrow \text{LUMO}$. The first two transitions were expected at lower energy than the latter. Figure 8a displayed two absorption bands at 1139 and 952 nm that may have been due to the transition expected at higher energy.

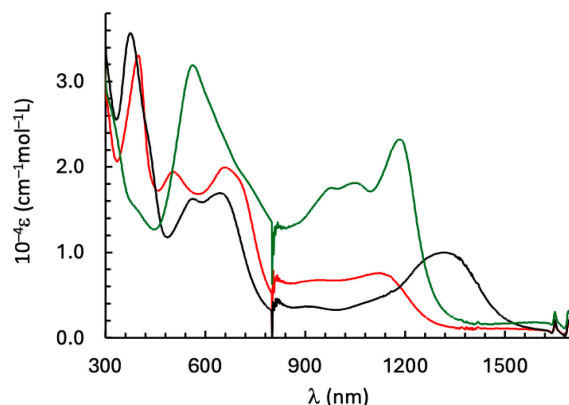


Figure 7. Electronic absorption spectra of Co_3HHTP (red trace), the one-electron reduced species (black trace) and the one-electron oxidized species (green trace) in dichloromethane.

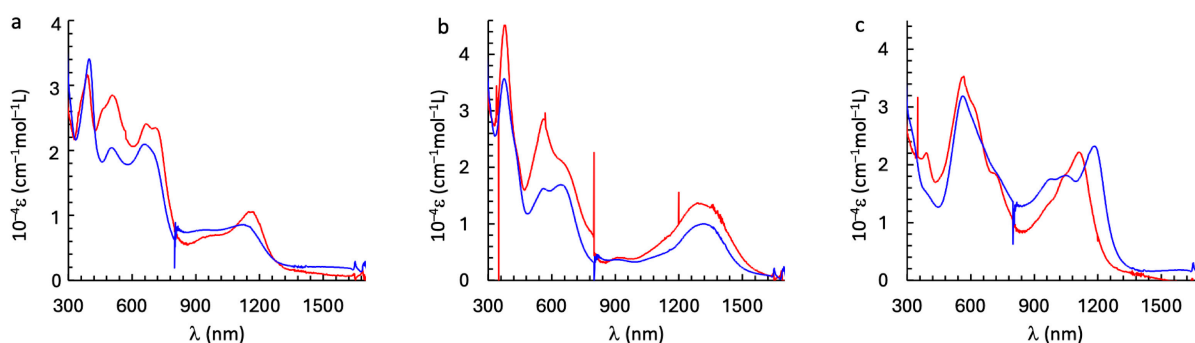


Figure 8. Electronic spectra recorded in UV-vis-NIR spectroelectrochemistry experiments for (a) **1** and Ni_3HHTP , (b) the one-electron reduced species and (c) the one-electron oxidized species, blue and red traces for the Co- and Ni-containing species, respectively, in dichloromethane containing 0.1 M $[\text{Bu}_4\text{N}]\text{PF}_6$ at 25 °C.

The spectra of the one-electron reduced species (Figure 8b) were also very similar in the NIR region, confirming that these transitions were mainly centered on the bridging ligand that was in the [sq-sq-cat] state and that the nature of the metal ions did not have a significant effect on the electronic structure of the bridging ligand. The situation was different for the one-electron oxidized species (Figure 8c), where a blue-shift of 60 nm (468 cm^{-1}) was observed for the most intense band when going from the Co to the Ni-containing complexes. The analysis performed here was only qualitative. A better understanding of the impact of the metal ions on the optical properties of the trinuclear species and their redox behavior requires an assignment of the different absorption bands that can be eventually performed with the help of time-dependent density functional calculations that are underway.

3.4. Magnetic Properties

The magnetic properties of Co_3HHTP were investigated by measuring the thermal dependence of the χT product (Figure 9a) and the magnetization vs. the magnetic field at $T = 2, 4, 6\text{ K}$ (Figure 9b). The value of the χT product at $T = 300\text{ K}$ ($8.51\text{ cm}^3\text{mol}^{-1}\text{K}$) may have corresponded to one $s = 1/2$ with $g = 2$ and three $s = 3/2$ with $g = 2.4$ non-interacting species. Such a g value for Co(II) is not unreasonable. Upon cooling, χT decreased monotonically until a value of $7.5\text{ cm}^3\text{mol}^{-1}\text{K}$ at $T = 75\text{ K}$ and then more abruptly. It reached a value of $3\text{ cm}^3\text{mol}^{-1}\text{K}$ at 2 K . The relatively large χT value at low temperature indicated a magnetic ground state and the decrease an antiferromagnetic coupling with certainly magnetic anisotropy, as indicated from theoretical calculations. The

$M = f(B/T)$ curves were not superimposable, which confirmed the presence of magnetic anisotropy within the complex.

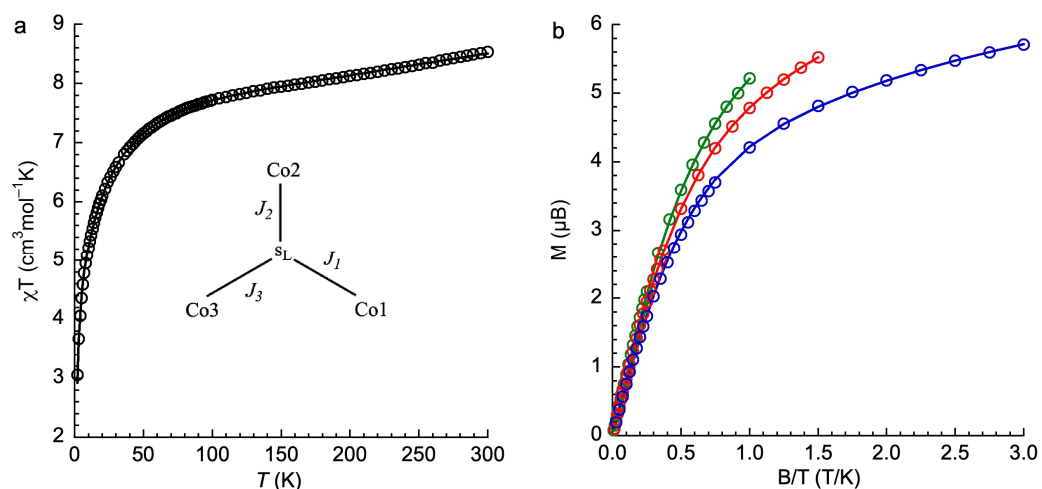


Figure 9. $\chi T = f(T)$ plot and exchange coupling scheme (a) and $M = f(B/T)$ plots at $T = 6$ (green), 4 (red) and 2 (blue) K (b) for Co_3HHTP ; experimental data (\circ) and fit (—) with the parameters in Table 4.

Table 4. Magnetic data fit parameters for Co_3HHTP . The ZFS and the exchange parameters in cm^{-1} .

$g_1 = g_2 = g_3$	$D_1 = D_3$	D_2	$E_1 = E_3$	E_2	$J_1 = J_3$	J_2	TIP
2.55(2)	−22(2)	−60(3)	3.3(3)	6.7(5)	−0.1	−129(4)	1.1×10^{-3}

The data were fitted using PHI [19], assuming a model with a central $s = 1/2$ and three peripheral $s = 3/2$ spins introducing TIP in the fit procedure. The number of parameters was large (three g values, six ZFS parameters and three exchange coupling parameters). We therefore proceeded in several steps in order to delimit the values of the different parameters and relied on theoretical calculation by considering one large antiferromagnetic exchange coupling and two very weak, on one hand, and on the other hand, we assumed first the same or very close ZFS parameters for the three Co(II) species. Considering this last assumption, it was not possible to reach a satisfactory solution. We therefore used different ZFS parameters but still negative ones because distorted pentacoordinate Co(II) complexes were found to have negative D values in many cases [17,20–22]. The best fit parameters are given in Table 4.

Overall, the parameters that best fit the magnetic data were qualitatively in agreement with those extracted from calculations, even though the figures may have differed when we examined those corresponding to each Co(II) species. There was a large antiferromagnetic exchange coupling between the unpaired electron of HHTP and *one* of the Co(II) species and two very weak couplings with the two other Co(II), as calculations predicted. The axial ZFS D values were all negative, but we found weaker values (in absolute value) for two Co(II), while for the third Co(II) the D value was almost the same as that extracted from calculations. The rhombic ZFS parameters of E found from the fit were weaker than those evaluated from calculations.

4. Conclusions

We report the preparation, under aerobic conditions, of a trinuclear Co(II)-containing complex using the tris-dioxolene triphenylene bridging ligand (HHTP). The crystal structure analysis and particularly the C–O bond distances of the OCCO moieties of the ligand suggested that HHTP was in the [sq-sq-sq] state even when the synthesis was carried out starting from the tris-catecholate species. The cyclovoltammetry study confirmed that, in

solution, the complex remained in the [sq-sq-sq] state with four accessible species, namely [cat-cat-cat], [cat-cat-sq], [cat-sq-sq] and [sq-sq-sq]. The spectroelectrochemical studies of Co_3HHTP and Ni_3HHTP indicated that, qualitatively, the electronic structure of HHTP was independent of the nature of the metal ions for the [cat-sq-sq], and the [sq-sq-sq] states. Ab initio calculations were consistent with a strong antiferromagnetic exchange coupling among the three unpaired electrons of the HHTP and led to a ground doublet state localized mainly on one OCCO moiety close to one of the three peripheral Co(II) complexes, as already found for Ni_3HHTP . Consequently, the magnetic properties were the result of a large antiferromagnetic exchange coupling with one Co(II) and much weaker couplings with the other two. The main difference in the magnetic properties between **1** and Ni_3HHTP was that the two weak exchange coupling parameters were much weaker for Co_3HHTP than for Ni_3HHTP (less than 1 cm^{-1} for Co_3HHTP and larger than 20 cm^{-1} for Ni_3HHTP [7]), as found from fitting the magnetic data. This was due to the larger localization of the central doublet of HHTP for Co_3HHTP than for Ni_3HHTP (Figure 10a,b)). This larger localization stemmed from a larger distortion of the HHTP skeleton in Co_3HHTP than in Ni_3HHTP (Figure 10c,d).

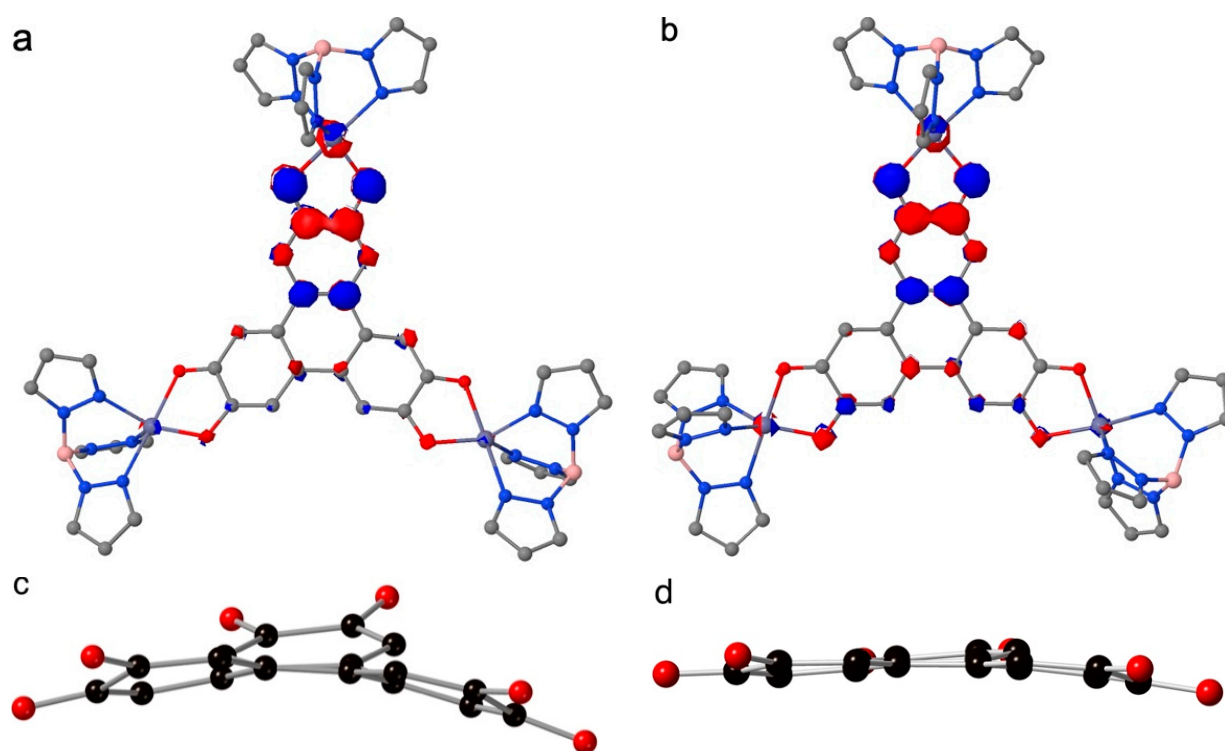


Figure 10. Representation of the SOMOs of the model complexes Zn_3HHTP for Co_3HHTP (a) and for Ni_3HHTP (b), where a larger localization of the orbital can be observed for Co_3HHTP ; and view of the geometry of HHTP for the two complexes with the central cycle of HHTP perpendicular to the plane, highlighting its larger distortion for Co_3HHTP (c) than for Ni_3HHTP (d).

Supplementary Materials: The following supporting information can be downloaded at: <https://www.mdpi.com/article/10.3390/magnetochemistry10120102/s1>, Figure S1: An ORTEP drawing of compound Co_3HHTP . Thermal ellipsoids are shown at the 30% level. Solvent molecules ($\text{C}_3\text{H}_6\text{O}$ & H_2O) were omitted for clarity. Hydrogen atoms are omitted for clarity; Figure S2: Molecular orbitals localized on the Co calculated for Co_3HHTP at the CAS(12,12)SCF level; Table S1: Crystallographic data and structure refinement details for Co_3HHTP ; Table S2: Energy spectrum of Co_3HHTP obtained from CAS(12/12)SCF + NEVPT2 calculations; Table S3: Contribution to D of the first four excited states for the Co2 magnetic center. The occupation of the orbitals in the dominant determinants of each state are given for the following orbital sequence $|z^2\ xz\ yz\ x^2 - y^2\ xy|$ followed by their

weight in the CAS(7,5) wave function. Determinants contributing to less than 10% are not reported. GS = ground state, ESi = excited states numbering $i = 1$ to 4; Table S4: Contribution to D of the first four excited states for the Co1 magnetic center. The occupation of the orbitals in the dominant determinants of each state are given for the following orbital sequence $|z^2 \ xz \ yz \ x^2 - y^2 \ xy|$ followed by their weight in the CAS(7,5) wave function. Determinants contributing to less than 10% are not reported. GS = ground state, ESi = excited states numbering $i = 1$ to 4; Table S5: Anodic (E_a) and cathodic (E_c) peak potentials, half-wave potentials and differences of the half-wave potentials from the CV of Ni₃HHTP and for Co₃HHTP.

Author Contributions: Conceptualization, T.M.; synthesis, A.C., Y.W. and F.L.; theory, N.S. and N.G.; crystallography, R.G.; magnetic study and analysis, E.R. and A.C., electrochemistry, and optical measurements, A.C. and Z.H.; data analysis, A.C., Y.W. and N.B.; supervision, N.B., F.L. and S.-i.O.; writing—original draft, T.M.; writing—reviewing and editing, N.B., Z.H., N.G., T.M. and S.-i.O. All authors have read and agreed to the published version of the manuscript.

Funding: This work is supported by the ADI 2021 project funded by the IDEX Paris-Saclay, ANR-11-IDEX-0003-02 and JST SPRING (JPMJSP2108). This work was also supported by the ANR (project SMOLMAGIQ ANR-20-CE29-0010) and Grant-in-Aid for Scientific Research (A) from the Japan Society for the Promotion of Science (JSPS) (20H00369).

Data Availability Statement: The original contributions presented in the study are included in the article/Supplementary Materials. Further inquiries can be directed to the corresponding author.

Acknowledgments: A.C. acknowledge the University Paris-Saclay and the University of Tokyo for financial support within the framework of the double diploma agreement. The authors thank the CNRS (Centre de la Recherche Scientifique) for financial support.

Conflicts of Interest: The authors declare no conflicts of interest.

References

1. Barthram, A.M.; Cleary, L.; Kowallick, R.; Ward, M.D. A new redox-tunable near-IR dye based on a trinuclear ruthenium(II) complex of hexahydroxytriphenylene. *Chem. Commun.* **1998**, *126*, 2695–2696. [[CrossRef](#)]
2. Ward, M.D.; McCleverty, J.A. Non-innocent behaviour in mononuclear and polynuclear complexes: Consequences for redox and electronic spectroscopic properties. *J. Chem. Soc. Dalton Trans.* **2002**, *3*, 275–288. [[CrossRef](#)]
3. Grange, C.S.; Meijer, A.J.H.M.; Ward, M.D. Trinuclear ruthenium dioxolene complexes based on the bridging ligand hexahydroxytriphenylene: Electrochemistry, spectroscopy, and near-infrared electrochromic behaviour associated with a reversible seven-membered redox chain. *Dalton Trans.* **2010**, *39*, 200–211. [[CrossRef](#)] [[PubMed](#)]
4. Wang, Y.T.; Lambert, F.; Rivière, E.; Guillot, R.; Herrero, C.; Tissot, A.; Halime, Z.; Mallah, T. Electronic and spin delocalization in a switchable trinuclear triphenylene trisemiquinone bridged Ni complex. *Chem. Commun.* **2019**, *55*, 12336–12339. [[CrossRef](#)] [[PubMed](#)]
5. Yang, L.M.; He, X.; Dinca, M. Triphenylene-Bridged Trinuclear Complexes of Cu: Models for Spin Interactions in Two-Dimensional Electrically Conductive Metal-Organic Frameworks. *J. Am. Chem. Soc.* **2019**, *141*, 10475–10480. [[CrossRef](#)] [[PubMed](#)]
6. Yang, L.M.; Dinca, M. Redox Ladder of Ni Complexes with Closed Shell, Mono-, and Diradical Triphenylene Units: Molecular Models for Conductive 2D MOFs. *Angew. Chem. Int. Ed.* **2021**, *60*, 23784–23789. [[CrossRef](#)]
7. Suaud, N.; Colin, A.; Bouammali, M.; Mallah, T.; Guihéry, N. Understanding the Electronic Structure of Magnetic Trinuclear Complexes Based on the Tris-dioxolene Triphenylene Non-innocent Bridging Ligand, a Theoretical Study. *Chem. Eur. J.* **2024**, *30*, e202302256. [[CrossRef](#)]
8. Suenaga, Y.; Inada, H.; Inomata, M.; Yamaguchi, R.; Okubo, T.; Maekawa, M.; Kuroda-Sowa, T. Crystal Structure and Characterization of Trinuclear Cobalt(III) Complex with 2,3,6,7,10,11-Hexahydroxytriphenylene. *Chem. Lett.* **2014**, *43*, 562–564. [[CrossRef](#)]
9. Uehara, K.; Hikichi, S.; Akita, M. Highly labile cationic tris-acetonitrile complexes, [TpM(NCMe)]OTf (M = Ni, Co; Tp: Hydrotrispyrazolylborato, R = Ph, Me and iPr): Versatile precursors for Tp-containing nickel and cobalt complexes. *J. Chem. Soc. Dalton Trans.* **2002**, 3529–3538. [[CrossRef](#)]
10. Sheldrick, G.M. *SHELXS-97, Program for Crystal Structure Solution*; University of Göttingen: Göttingen, Germany, 1997.
11. Sheldrick, G. A short history of SHELX. *Acta Cryst. Sec. A* **2008**, *64*, 112–122.
12. Farrugia, L.J. WinGX suite for small-molecule single-crystal crystallography. *J. Appl. Cryst.* **1999**, *32*, 837. [[CrossRef](#)]
13. Neese, F.; Wennmohs, F.; Becker, U.; Riplinger, C. The ORCA quantum chemistry program package. *J. Chem. Phys.* **2020**, *152*, 224108. [[CrossRef](#)]
14. Malmqvist, P.Å.; Roos, B.O.; Schimmelpfennig, B. The restricted active space (RAS) state interaction approach with spin-orbit coupling. *Chem. Phys. Lett.* **2002**, *357*, 230–240. [[CrossRef](#)]

15. Addison, A.W.; Rao, T.N.; Reedijk, J.; Vanrijn, J.; Verschoor, G.C. Synthesis, Structure, and Spectroscopic Properties of Copper(II) Compounds Containing Nitrogen Sulfur Donor Ligands—The Crystal and Molecular-Structure of Aqua[1,7-Bis(N-Methylbenzimidazol-2'-yl)-2,6-Dithiaheptane]Copper(II) Perchlorate. *J. Chem. Soc. Dalton Trans.* **1984**, *7*, 1349–1356. [[CrossRef](#)]
16. Maurice, R.; Bastardis, R.; de Graaf, C.; Suaud, N.; Mallah, T.; Guihéry, N. Universal Theoretical Approach to Extract Anisotropic Spin Hamiltonians. *J. Chem. Th. Comput.* **2009**, *5*, 2977–2984. [[CrossRef](#)]
17. Gomez-Coca, S.; Cremades, E.; Aliaga-Alcalde, N.; Ruiz, E. Mononuclear Single-Molecule Magnets: Tailoring the Magnetic Anisotropy of First-Row Transition-Metal Complexes. *J. Am. Chem. Soc.* **2013**, *135*, 7010–7018. [[CrossRef](#)]
18. Ruamps, R.; Batchelor, L.J.; Maurice, R.; Gogoi, N.; Jiménez-Lozano, P.; Guihéry, N.; de Graaf, C.; Barra, A.L.; Sutter, J.P.; Mallah, T. Origin of the Magnetic Anisotropy in Heptacoordinate Ni and Co Complexes. *Chem. Eur. J.* **2013**, *19*, 950–956. [[CrossRef](#)] [[PubMed](#)]
19. Chilton, N.F.; Anderson, R.P.; Turner, L.D.; Soncini, A.; Murray, K.S. PHI: A powerful new program for the analysis of anisotropic monomeric and exchange-coupled polynuclear d- and f-block complexes. *J. Comput. Chem.* **2013**, *34*, 1164–1175. [[CrossRef](#)]
20. Ruamps, R.; Batchelor, L.J.; Guillot, R.; Zakhia, G.; Barra, A.L.; Wernsdorfer, W.; Guihéry, N.; Mallah, T. Ising-type magnetic anisotropy and single molecule magnet behaviour in mononuclear trigonal bipyramidal Co(II) complexes. *Chem. Sci.* **2014**, *5*, 3418–3424. [[CrossRef](#)]
21. Cahier, B.; Perfetti, M.; Zakhia, G.; Naoufal, D.; El-Khatib, F.; Guillot, R.; Rivière, E.; Sessoli, R.; Barra, A.L.; Guihéry, N.; et al. Magnetic Anisotropy in Pentacoordinate Ni and Co Complexes: Unraveling Electronic and Geometrical Contributions. *Chem. Eur. J.* **2017**, *23*, 3648–3657. [[CrossRef](#)]
22. Devkota, L.; SantaLucia, D.J.; Wheaton, A.M.; Pienkos, A.J.; Lindeman, S.V.; Krzystek, J.; Ozerov, M.; Berry, J.F.; Telser, J.; Fiedler, A.T. Spectroscopic and Magnetic Studies of Co(II) Scorpionate Complexes: Is There a Halide Effect on Magnetic Anisotropy? *Inorg. Chem.* **2023**, *62*, 5984–6002. [[CrossRef](#)] [[PubMed](#)]

Disclaimer/Publisher's Note: The statements, opinions and data contained in all publications are solely those of the individual author(s) and contributor(s) and not of MDPI and/or the editor(s). MDPI and/or the editor(s) disclaim responsibility for any injury to people or property resulting from any ideas, methods, instructions or products referred to in the content.